Title	Single-walled carbon nanotube membrane accelerates active osteogenesis in the bone defect. : the possibility for guided bone regeneration membrane
Author(s)	,
Citation	. ( ) 14993
Issue Date	2022-03-24
DOI	10.14943/doctoral.k14993
Doc URL	http://hdl.handle.net/2115/89307
Type	theses (doctoral)
File Information	Xu_Yikun.pdf

Instructions for use

博 士 論 文

Single-walled carbon nanotube membrane accelerates active osteogenesis in the bone defect. -the possibility for guided bone regeneration membrane-

（単層カーボンナノチューブを用いた

骨誘導再生膜の開発と骨再生能の評価）

令和４年３月申請

北海道大学

大学院歯学院口腔医学専攻

徐 易 坤

Introduction

Carbon nanotubes (CNTs) are sp[2] carbon bonded tubular materials reported by Iijima et al. [1,2]. There are two main types of CNTs, single-walled carbon nanotubes (SWCNTs) and multi-walled carbon nanotube (MWCNT). CNTs have been extensively studied in the biomedicine field because of their physical and chemical properties, unique structure, biocompatibility, and low toxicity [3–7]. Usui et al.[8] revealed that MWCNTs could accelerate bone formation and show high bone tissue compatibility. Barrientos-Durán et al.[9] revealed that human preosteoblasts and murine embryonic stem cells osteogenic differentiation were accelerated by culturing on SWCNTs. We previously reported that multi-walled CNT (MWCNT)-coated substrates can be effective for adhesion and differentiation of osteoblasts and have a favorable compatibility profile for bone[10–12]. MWCNTs-coated collagen sponges could be loaded with growth factors to achieve controlled release and promote bone regeneration[13].

The guided bone regeneration (GBR) technique is one of the most commonly applied methods to reconstruct alveolar bone and treat peri-implant bone defects. For the GBR technique, a barrier membrane is used to cover the bone defects, preventing the entry of non-osteogenic cells like epithelial cells and fibroblasts in bone defects[14–16]. The membrane should also maintain space for new bone formation.

Murray et al. reported that shielding the bone defect from the surrounding tissue accelerates bone healing[17]. GBR technique is widely used for maxillofacial area and the materials of the membranes used for the GBR technique have been actively researched. The required properties for GBR membranes are biocompatibility, mechanical strength, and surgical maneuverability[14]. The following materials have been studied as GBR membranes: natural polymers such as collagen, chitosan, and silk fibroin; metals such as titanium alloys, magnesium alloys, and zinc alloys; and synthetic polymers such as polytetrafluoroethylene (PTFE). However, PTFE as the non-resorbable material does not have sufficient strength and hydrophilic characteristics that could be treated with protein such as growth factor. On the other hand, collagen and chitosan as resorbable materials have insufficient strength and sometimes cause inflammation on the resorption. Therefore, these materials sometimes delay bone regeneration in clinical practice because of their insufficient mechanical and biological properties[17,18].

To develop GBR membranes, we previously prepared carbon nanohorns (CNHs), a type of carbon nanomaterial, and adhered CNHs to PTFE membranes and evaluated their bone regenerative ability. The membranes with CNHs promoted bone regeneration[19], and CNHs accelerated osteoblast differentiation via macrophage activation[20]. On the other hand, the strength of the CNH membranes was weak due to their adherence to PTFE membranes, and some CNHs detached from the membrane surface. Therefore, we proposed that these problems could be improved by using single-walled CNTs (0.5-2.0 nm in diameter and more

than 100 nm to several centimeters in length) with the characteristic nanostructured surface, high mechanical strength and a large surface area[21,22] as independent membranes without lining such as PTFE. In the present study, SWCNTs dispersed in hyaluronic acid (HA) were prepared as HACNT membrane and observed its morphological structure and mechanical properties. In addition, we investigated the inhibition of non-osteogenic cell proliferation and the promotion of osteoblast proliferation, which are essential factors for the success of the GBR method. Then, the tissue response and bone regeneration ability were evaluated, and the dispersion of CNTs in surrounding tissues was surveyed using a Raman spectroscopy. The present study demonstrates that the HACNT membrane showed high strength and hydrophilicity and inhibited non-osteogenic cell proliferation but promoted osteoblast proliferation. Furthermore, extensive osteogenesis in bone defects in the rat calvaria was observed, whereas the CNT was scarcely diffused in the tissue around the membrane.

Materials & Methods

Preparation of HACNT membrane

Single-walled carbon nanotubes (MEIJO eDIPS 1.5p, Japan) were dispersed in 0.1mg/mL hyaluronic acid (FUJIFILM, Japan) solution at 0.5mg/mL by bath sonication for 30 minutes and a homogenizer at Amp 50%, 1sec/1sec, 10min, total 20min. The suspension was filtrated by a filter membrane (Omnipore, 0.1μm pore, 47mm diameter) and dried in a 60°C dry oven. The Hyaluronic acid single-walled carbon nanotubes (HACNT) membranes were stripped from the filter membranes, then hydrophilic treated by UV ozone cleaner (PC450, Meiwa fosis, Japan) for 10 minutes.

Characterization of HACNT membrane

The HACNT membranes were observed by scanning electron microscope at 10kV (SEM, S-400, Hitachi, Tokyo, Japan). The contact angle was measured by Phoenix Alpha P200 (Meiwa fosis, Japan). For the mechanical strength test, a dumb-bell shape SWCNT membrane was made with 2 mm width at middle and stretched by MST-I type HS/HR (Shimadzu, Japan) with a 25 N load cell, and PTFE membranes were also measured in the same method for comparison. The membrane thickness was measured with a constant pressure thickness gauge (PG-02, TECLOCK, Japan).

Quantifying the volume of hyaluronic acid in the HACNT membrane

The amount of hyaluronic acid contained in HACNT membrane was calculated form the concentration of hyaluronic acid in the filtrated solution. Absorption spectrum of both the filtrated solution and 0.1mg/ml hyaluronic acid were measured by optical absorption spectrometer and compared.

Measurement of elution of HACNT membranes into PBS

HACNT (1.0 mg) membranes were immersed in 10 ml of PBS and allowed to stand for 8 weeks at room temperature and pressure. Ten ml of PBS without CNTs was used as a control. Five ml of the PBS solution after removing the CNT membranes was dispensed into a separate vial, 50 mg of SDBS was added, and the solution was dispersed by bath sonication for 30 min. The absorption spectra of both sample and control groups were measured by optical absorption spectrometer (UV-3100, Shimadzu, Japan) and compared.

In vitro experiments

Cell culture on HACNT membrene

Mouse calvaria osteoblastic cell line (MC3T3-E1)[23], human gingival carcinoma epithelial-like cells (Ca9-22)[24] were culture in Minimum Essential Medium Eagle (Sigma-Aldrich, St. Louis, MO, USA) containing 10% fetal bovine serum (CELLECT,

France), 2mM Glutamine, and 1% penicillin/streptomycin (Thermo Fischer Scientific, Gibco, Waltham, MA) at 50 U/mL penicillin and 50 mg/mL streptomycin. Mouse embryonic fibroblasts cell line (NIH/3T3)[25] were cultured in Dulbecco's Modified Eagle's Medium-high glucose(Sigma-Aldrich, St. Louis, MO, USA) containing 10% calf serum (Funakoshi, Japan) and 1% penicillin/streptomycin (Thermo Fischer Scientific, Gibco, Waltham, MA) at 50 U/mL penicillin and 50 mg/mL streptomycin. All cells were cultured at 37C with a 5% CO_2 atmosphere.

For evaluation of each cells proliferation on the HACNT membrane, the HACNT membranes were placed at the bottom of 48-well-plate (Corning, Kennebunk, ME, USA), and 500 μL of 3 kinds of cell suspension at 2×10^4 cells/mL were seeded on the HACNT membranes or blank wells as the control for 3 and 7 days (n=6).

Cell culture in the presence of HA

Mouse bone marrow stromal cells (mBMSCs, ATCC) were cultured in Dulbecco's Modified Eagle's Medium-high glucose (Sigma-Aldrich, St. Louis, MO, USA) containing 10% fetal bovine serum (Funakoshi, Japan) and 1% penicillin/streptomycin (Thermo Fischer Scientific, Gibco, Waltham, MA) at 50 U/mL penicillin and 50 mg/mL streptomycin. All cells were cultured at 37℃ with a 5% CO_2 atmosphere.

For evaluation of each cells proliferation and ALP activity in different concentrations of hyaluronic acid solution. Cells were suspended in 500 μL culture medium with 0, 0.05, 0.1, 0.5mg/mL hyaluronic acid solution and seeded in a density of 1×10^4 cells/mL in 48-well-plate (Corning, Kennebunk, ME, USA) for 7 days (n=5).

SEM observation

After 3 days, we observed the cells on the HACNT membranes by SEM, where the samples were washed three times with phosphate-buffered saline and fixed with 2.5% glutaraldehyde. After dehydration through a graded ethanol series, they were dried using the critical point method and sputter coated with palladium-platinum for SEM observation.

DNA content quantification

After 3 and 7 days of cultivation, the wells and HACNT membranes were washed with PBS. 300 μL of the 0.2% IGEPAL CA630 (Sigma-Aldrich, MO, USA) was added to each well. The samples were frozen, thawed, and then homogenized. The sample solution was added to 100 mL of 4M NaCl, 0.1M phosphate buffer (pH 7.4), and then centrifuged for DNA analysis. Picogreen (Thermo Fischer Scientific, Waltham, MA) was used to measure the DNA content via a fluorometer (Infinite F200 PRO, Tecan, Switzerland) with the excitation filter set at 356nm and the emission filter at 458 nm.

Alkaline Phosphatase activity measurement

Alkaline phosphatase (ALP) activity was measured with LabAssay (Wako, Japan). Twenty microliters of the supernatant fluid in the sample were added to 100 μL of p-nitrophenol phosphate in carbonate buffer and incubated for 15 min at 37°C. After 80 μL of NaOH was added, absorbance was measured at 405 nm using the fluorometer (Infinite F200 PRO, Tecan, Switzerland) and enzyme activity was determined from the calibration curve p-nitrophenol standard. ALP activity was normalized by DNA content.

Animal experiments

For investigation of new bone regeneration for HACNT membrane, Wistar rats with calvarial defects were used as an animal model. All animal experiments received approval and were performed by the regulations from the Animal Care and Use Committee of Hokkaido University (No. 19-0061).

Bone regeneration evaluation

10-weeks-old Wistar male Rats (about 300g; CLEA Japan Inc., Tokyo, Japan) were inhalation anesthetized with isoflurane (Pfizer Inc., New York, NY, USA) and shaved the hair, and sterilized with 70% ethanol of the calvarial region. A semicircular incision was made on the rats scalp, separating skin and periosteum, exposing the calvarial bone by blunt dissection. An 8 mm diameter bone defect was made on exposed calvarial bone by a 7/8 mm diameter trephine bur (Stoma, Germany), covered the defect with a 12mm diameter HACNTor left untreated as control (n=6). After 8 weeks, rats were inhalation anesthetized with isoflurane and perfusion fixation by fixation solution (2.5% glutaraldehyde with 0.1M HEPES).

The samples containing the rats calvarial bone and membranes were harvested and fixed in fixation solution. For the radiographic evaluation, the samples were scanned by using microcomputed tomography (μ-CT, CosmoScan, Rigaku). The acquired CT photographs of samples were imported into Fuji ImageJ software, the 3D script plugin was used to 3D reconstruct and evaluate the samples. Materialize mimics version 21.0 software also used to calculate the new bone volume in the defect area[26], and the bone volume in surgically made defect area was calculated as new regenerated bone volume.. Then, the samples were also used for histological evaluation. The samples were resin embedded, sliced into 30-40 μm specimens in a coronal plane, stained by toluidine blue, observed by an optical microscope.

Statistical analysis

The bone volume of each group was compared by the Mann-Whitney test. The DNA content on the membrane was analyzed by a two-way ANOVA test and sidak's correction. Statistical significance was established at $P < 0.05$.

Raman Imaging

The micro-Raman mapping was carried out using a Renishaw inVia confocal microscope equipped with a 785-nm laser excitation source as previousry reported[27]. The laser, attenuated to about 0.5 mW, was focused on the sample surface with a ×50 objective lens with an NA of 0.75. The spot size was estimated to be about 0.87 μm. This size mainly determines the spatial resolution of the Raman images. The Raman signals from the sample were measured with an electron multiplying CCD detector (Andor) through a grating with 1200 grooves/mm. The step size of the measurements was 1.0 μm. The CCD integration time was 0.05 second for all measurements. The Raman spectra were fitted using a Lorenz function, and the Raman images were obtained by plotting the peak area intensities of the fitting results.

Results

Characterization of the HACNT membrane

Figure 1 (a-e) shows the characterization of the HACNT membrane. The HACNT film was a black independent film, as shown in Figure 1(a). The nanostructured surface with the characteristic bundle structure of SWCNTs was observed by SEM in Figure 1(b).

Figure 1 (c) shows the photograph when the water contact angle (CA) of the HACNT membrane was measured. In addition, the tensile strength of the HACNT membrane is 202 N/mm^2 in Figure 1(e), while that of PTFE membrane is 32 N/mm^2 in Figure 1(d). These results demonstrated that the hydrophilicity and strength of the CNT membrane were much higher than those of the PTFE membrane.

This study used HA to disperse SWCNTs and bind them to finish the shape of the membrane. HA is known as a natural component of the human body. It has already been applied for drugs and biomaterials such as viscosupplementation and bioscaffold[28–30]. They have confirmed its safety. The HA content in the HACNT membrane could be calculated to 7.7wt% (Figure 1(f)).

Figure 1(g) shows that the amount of SWCNTs diffused from the CNT membrane is below the detection limit even after 8 weeks of immersion in PBS.

Cell proliferation on the HACNT membrane

The GBR membrane covering the bone defects needs to prevent the non-osteogenic cells such as epithelial cells and fibroblasts from invading bone defects while increasing the proliferation of the osteoblastic cells to form the new bone in the space under the membrene[14,15]. In this study, the proliferation of three types of cells was estimated. Figure 2 (Aa-c, Ba-c) shows the proliferation of the Mouse calvaria osteoblastic cell line (MC3T3-E1), mouse embryonic fibroblasts cell line (NIH/3T3) and human gingival carcinoma epithelial-like cells (Ca9-22). SEM observation showed that the pseudopodia of MC3TC-E1 were more extended and entangled to the CNT membrane than other types of cells (Figure 2Aa-c). Remarkably, on the HACNT membrane, osteoblasts showed a significant increase in cell number indicated by DNA content from 3 to 7 days (Figure 2Ba), while fibroblasts (Figure 2Bb) and epithelial cells (Figure 2Bc) did not show an increase in cell number.

Cell proliferation and differentiation in the presence of HA

Figure 2(C) shows the DNA content and alkaline phosphatase (ALP) activity of human mesenchymal stem cells cultured for 7 days in the presence of various concentrations of HA, and the DNA content and ALP activity did not have significant differences even when the concentration of hyaluronan at 0 ,0.05, 0.1 and 0.5 mg/mL.

Micro-CT analysis of the bone regeneration

Figure 3 shows the results of Micro-CT analyses of the bone regeneration in the calvarial

defect of rats covered with/without HACNT membrane after 8 weeks. As shown in Figure 3 (A), more extensive and higher radiopaque images were observed in the HACNT (Figures 3(A) b, d and f) membrane group compared to the control group without membrane (Figures 3(A), a, c and e). Figure 3B is a schematic of the measurement method for new bone in the defect area. The volume of new bone in the HACNT membrane group was significantly higher than that in the control group by Micro-CT analyses (Figure 3C).

Histology of the bone regeneration

Figure 4 shows the histology of the two groups, at 8 weeks, a new bone (black asterisk) was formed from the edge of the existing calvarial bone (EB). Some of the new bone was seen apart from the existing bone (Figure 4(A) a). Newly formed bone had lamellar structures (black arrow)(Figure 4(A) b). Fibrous connective tissue, including fibroblasts, was observed around the newly formed bone. These results indicated that bone regeneration in the control group had finished. On the other, more extensive bone formation was observed under the HACNT membrane (yellow arrowhead) (Figure 4(B) a) compared to the control group (Figure 4(A) a). A part of the HACNT membrane (pink arrowhead) was folded on a newly formed bone (Figure 4(B) a). Newly formed bone was formed continuously with the edge of the calvaria. Many osteoblasts (white arrowhead), cells with large light cytoplasm like mesenchymal cell (black arrowhead), and capillaries (white arrow) which showed active osteogenesis, were observed on the upper part of the newly formed bone (Figure 4(B) b). At the same time, the lamellar structure (black arrow) was seen only in the lower part of the newly formed bone along with the dura in (Figure 4(B) a). However, various types of cells such as like mesenchymal cells (black arrowhead), fibroblasts, macrophages, and capillaries (white arrow) were recognized under the HACNT membrane (Figure 4(B) c).Also, many cells with large cell bodies like mesenchymal cells (black arrowhead) were closed to the membrane.

Observation of the localization of SWCNTs by Raman imaging

There is a risk of diffusion of CNTs after being implanted in the body. Kang et al.[31] reported that the CNTs might cause cell damage through direct contact with the cell membrane. To further investigate the localization and state of SWCNT from the HACNT membrane, in this study, a resonance Raman mapping was carried out on the sections of bone tissue. Figure 5a and 5b show photographs of the histological sections of calvarial bone specimen implanted with HACNT membrane after 8 weeks with different magnifications. Figures 5d shows microscopic Raman mapping of calvaria bone tissue sections as shown in part in Figure 5a-c. Figure 5d maps the G-band intensity excited at 785nm overlaid in each point 1 (Figure 5f), point 2 (Figure 5g), and point 3 (Figure 5h). Table 5i shows the percentage of intensity at each

point, with the intensity of the HACNT membrane portion being 100%. In the bone tissue adjacent to the HACNT membrane, small amounts of SWCNTs were detected (Figure 5d).

Discussion

The surface properties of the material, including hydrophilicity and roughness, have a significant impact on cell proliferation and attachment[32]. Several studies have shown that hydrophilic surfaces can promote the growth, adhesion and proliferation of osteoblasts[32,33], fibroblasts[34] and epithelial cells[35]. The HACNT membrane consisted of 1.5 nm-diameter SWCNTs and the CA was 10°~ 16°, which means it has a specific nanostructure and high hydrophilicity. The characterizations were compared to the PTFE membrane because it has already used in clinic. Zhang et al. reported that the CA of PTFE is about 118° [36]. Even before oxidation, the CA of the HACNT film was 25° and further decreased after oxidation by treatment with UV ozone cleaner. The high hydrophilicity and the high degree roughness of the material surface promote the selective adsorption of fibrinogen and fibronectin, two critical regulators of osteoblast adhesion and proliferation[37,38]. However, in the present study, fibroblasts and epithelial cells on HACNT membranes did not increase as well as on cell culture dishes. Besides, the amount of DNA and ALP activity did not change in the presence of hyaluronan at concentrations estimated from the amount eluted from the membrane.

The difference in the proliferation of these cells on the HACNT membrane could be due to the surface roughness. It has been demonstrated that osteoblasts are likely to proliferate on rough surfaces[32], while fibroblasts and epithelial cells are likely to proliferate on smooth surfaces. Kunzler et al. reported that osteoblasts showed a significant increase in proliferation rate with increasing surface roughness. Fibroblasts showed the opposite proliferative behavior, with the proliferation rate decreasing with increasing roughness[39]. Baharloo et al. reported that epithelial cell proliferation decreased when seeded on a rough surface compared to a smooth surface[40]. Therefore, the hydrophilicity and specific nanostructure of HACNT membranes could promote cell adhesion and osteoblast proliferation, although the nanoscale surface structure might inhibit fibroblast and epithelial cell proliferation.

The HACNT membrane covered the bone defect made in rat calvaria. At 8 weeks after the surgery, the amounts of newly formed bone under the HACNT membrane were more than those in defects without membrane. Also, many osteoblasts, the cell like mesenchymal cell and capillaries indicating active osteogenesis were observed under the HACNT membrane, while only the lamellar structure were seen in the control group. Especially, many cells with large cell bodies like mesenchymal cells were closed to the membrane. These findings revealed that the high regenerative activity continues in the defects covered with the HACNT membrane even at the late stage of tissue repair. On the other hand, some of the HACNT membranes in the tissue were folded, and some fibrous connective tissue was observed between the membranes and bone. These results suggested that shielding ability could be improved by changing mechanical properties such as increasing the HACNT membranes flexibility. However, the selective proliferation of osteoblasts *in vitro* and extensive bone formation with the same thickness as the existing bone directly below the membrane was

observed, and also epithelial cells and fibroblasts did not proliferate while osteoblasts proliferated well on the HACNT membrane culture. Therefore, the HACNT membrane has enough shielding property to selectively proliferate osteoblasts and a high possibility of SWCNTs as a GBR membrane.

Previously, we reported the application of carbon nanohorns (CNH) for GBR membrane[19] and revealed that CNHs accelerate bone formation via macrophage activation[20]. The effect of CNH on bone formation was in the early stage of regeneration. However, these results would explain that the surface structure with specific nanostructure of SWCNTs of the membrane has another effect on bone formation especially in the late stage of regeneration. In this research, we proposed the new possibility of specific surface nanostructure by SWCNTs on bone formation. The new possibility of SWCNTs should be confirmed by further research in future.

Raman imaging suggested that the diffusion of CNT was scarcely observed around the membrane. Besides, the amount of SWCNTs diffused from the CNT membrane is below the detection limit even after 8 weeks of immersion in PBS. The Raman spectral data of SWCNTs around the new bone and the low solubility of HACNTs in PBS suggest that HACNT membranes are highly stable and hardly diffused after implantation. Moreover, in our previous study, SWCNTs were implanted between mices periosteum and parietal bone. SWCNTs appeared to be locally stable and had not dispersed to other organs[33]. However, we further validate the biocompatibility and dispersibility of this membrane consisting of SWCNTs.

Conclusions

The HACNT membrane showed high strength, hydrophilicity, stability (insolubility) and selective osteoblasts proliferation *in vitro* and continuously promoted bone formation by space-making and high osteogenic activity *in vivo*. Additionally, SWCNTs have the chemical property of absorbing proteins, allowing further development, such as loading growth factors and arranging toughness and morphology. Therefore, SWCNTs as independent membranes could be expected to be applied as GBR membranes to promote osteogenesis in cases of significant loss of both width and volume of alveolar bone due to defects caused by severely advanced periodontal disease, tooth loss, cancer and accidents. The results of this study will be an important milestone in creating a new design of therapeutic materials for bone regeneration using CNTs.

Figures
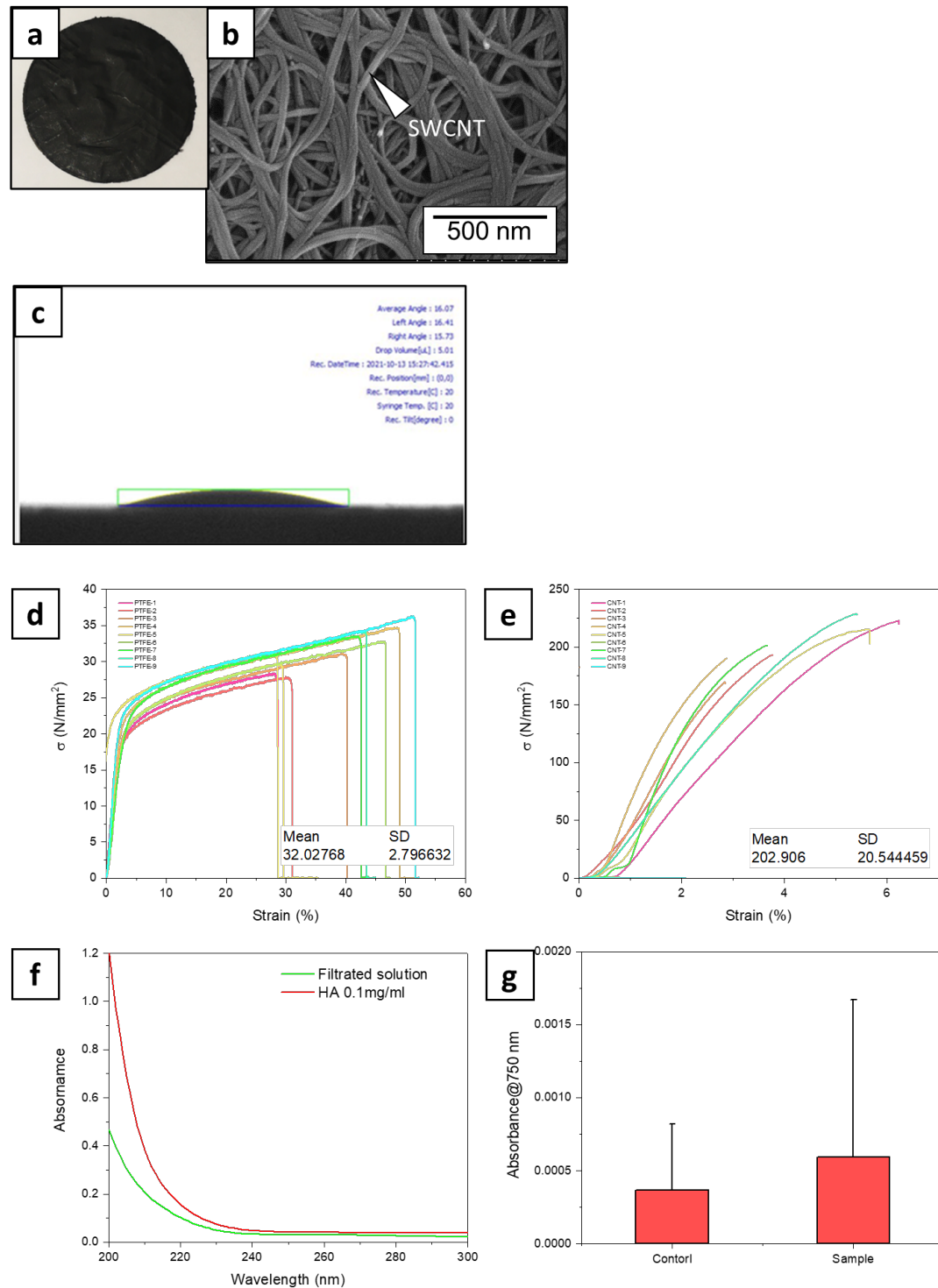
Figure 1. Characterization of HACNT membrane. (a) Photograph of HACNT membrane. (b) SEM image of HACNT membrane, the membrane consists of many bundles of SWCNT(arrowhead). (c) Images of the spreading of a water drop on the HACNT membrane. The average CA was about 16°. Graph of tensile strength of (d) PTFE membrane and (e) HACNT membrane. Mean tensile strength: (d)PTFE membrane=32 N/mm², (e)HACNT membrane: 203 N/mm² (n=9). (f) Absorbance of filtering solution of HACNT membrane, compared with 0.1mg/mL HA solution. (g) Absorbance of PBS solution with HACNT membrane immersed after 8 weeks at room temperature and pressure at the absorbance of 750 nm value (n=5).

14
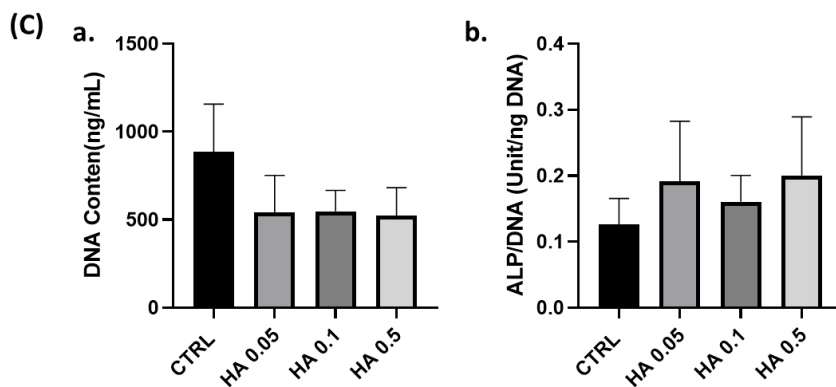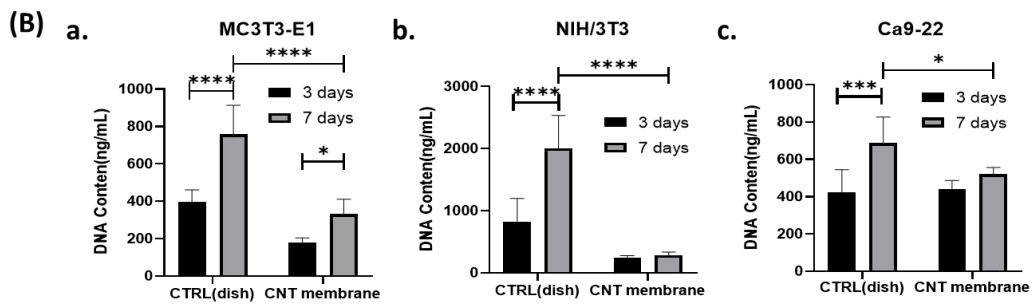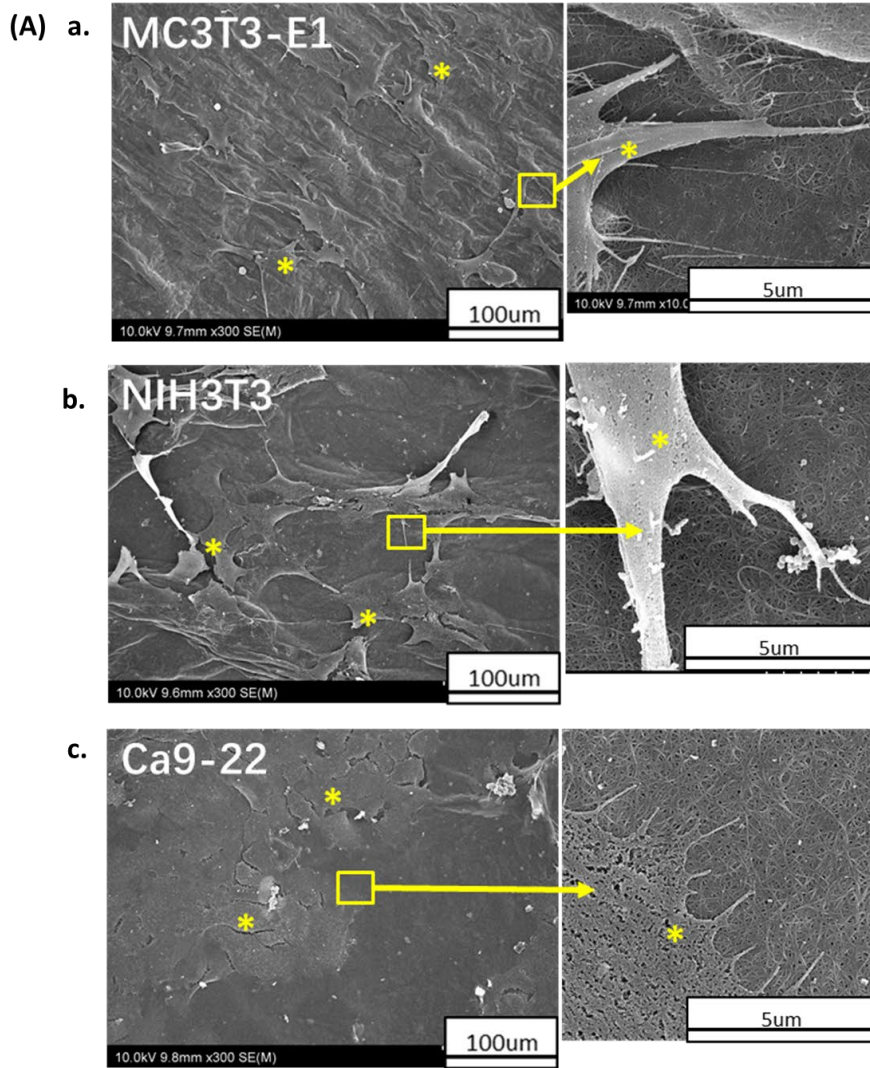
Figure 2. (A) SEM observations of MC3T3-E1(a), NIH3T3(b) and Ca9-22(c) cells cultured on HACNT membrane after 3 days(cells: yellow asterisk). **(B)** DNA contents of MC3T3-E1(a), NIH3T3(b) and Ca9-22(c) cells on HACNT membranes after 3 and 7 days culturing(n=6, *p<0.05, ***p<0.001, ****p<0.0001). **(C)** (a) DNA content and (b) ALP activity of mBMSCs cultured in culture medium with 0.05, 0.1. 0.5 mg/mL hyaluronic acid solution after 7 days (n=5).
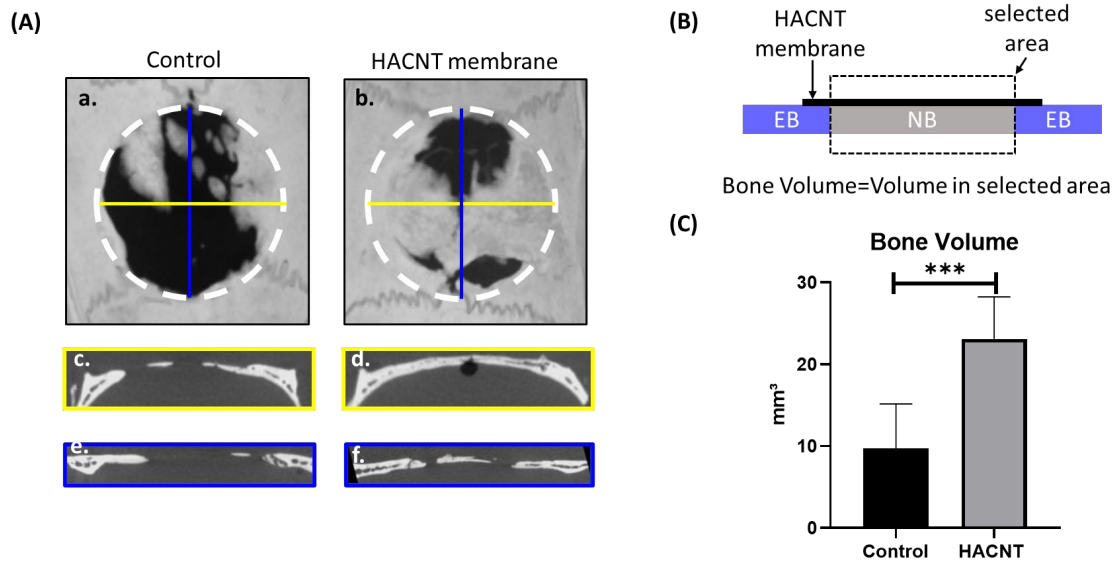
Figure 3. (A) Micro-CT images of representative rat's calvarial bone samples with/without HACNT implantation after 8 weeks. (a)(c)(e) Control (without membrane) and (b)(d)(f) HACNT membrane group were observed with 3 planes of direction: (a)(b) Horizontal plane. (c)(d)axial plane. (e)(f)sagittal plane. **(B)** Schematic of the measurement method of bone volume, new bone was defined as volume in the selected area. EB: Existing bone. NB: New bone. **(C)** Comparison of new bone volume regenerated in calvarial bone defect area of two groups. (n=6, ***p<0.001)
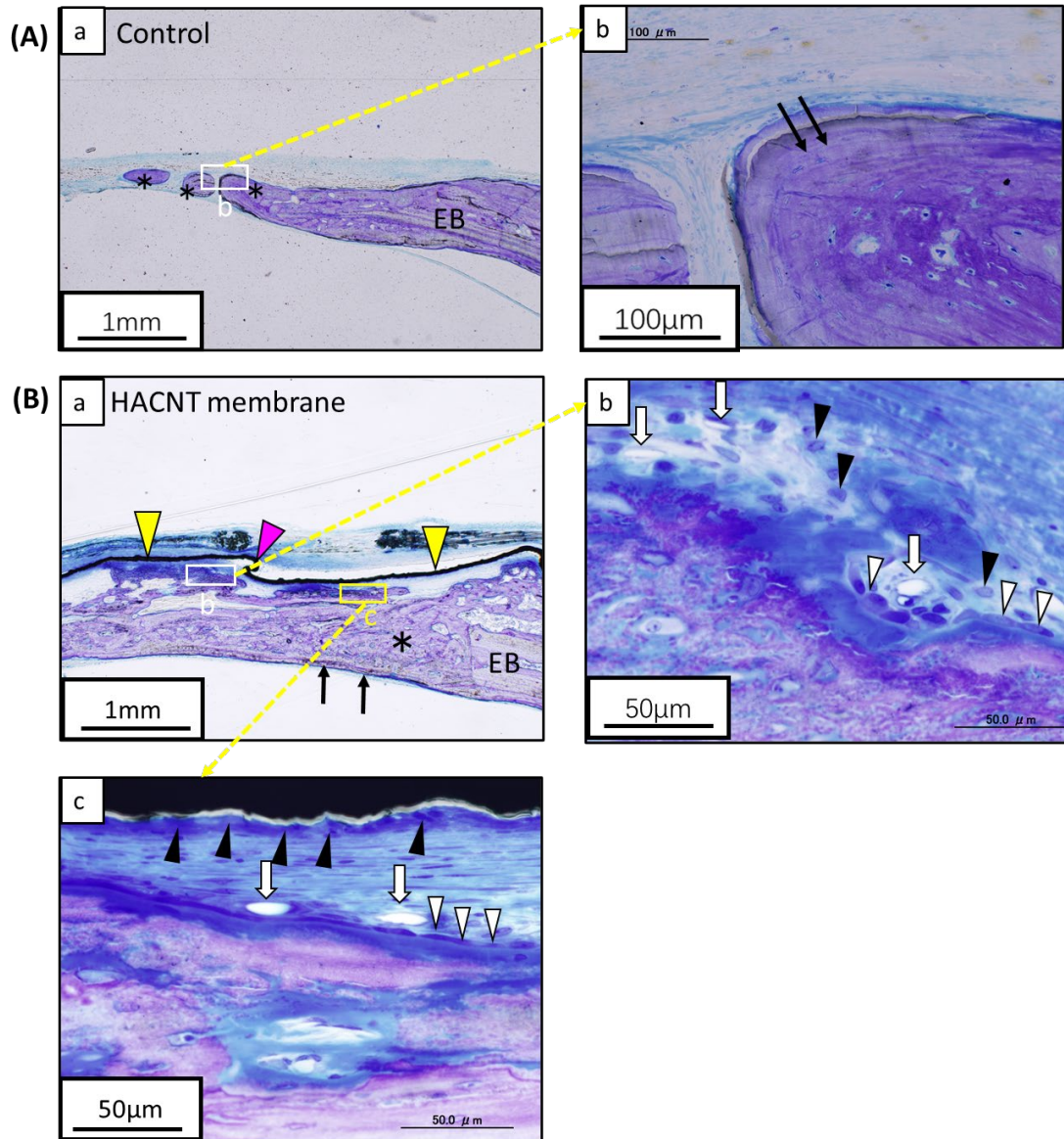
Figure 4. Representative histological sections of rat calvarial bone with/without HACNT implantation after 8 weeks.

(A) without membrane (control)   (a) Thick fibrous connective tissue covered the bone defect. New bone (black asterisk*) was formed in the defect. (b) High magnification of white square in (A, a) Lamellar structures (black arrow) were seen. **(B)** with HACNT membrane. (a) HACNT membrane (yellow arrowhead) covered bone newly formed bone (*) and existing bone (EB). A part of the membrane was folded(pink arrowhead) (b) High magnification of white square in (B, a). Active osteogenesis was seen in the upper part of the newly formed bone. Osteoblasts (white arrowhead) and cells with large body like mesenchymal cells (black arrowhead) were observed on new bone. (c) High magnification of yellow square of (B, a). Many cells with large body like mesenchymal cells (black arrowhead) were observed close to the HACNT membrane. Osteoblasts (white arrowhead) and capillaries (white arrow) indicating active osteogenesis were recognized.
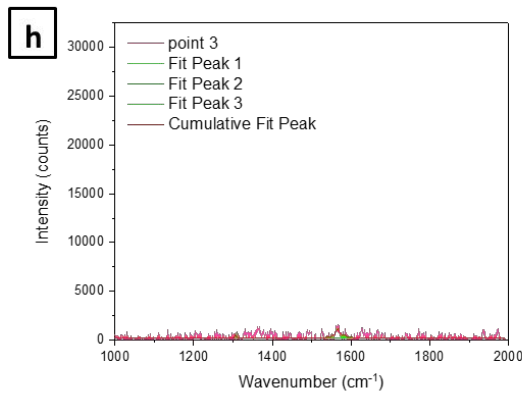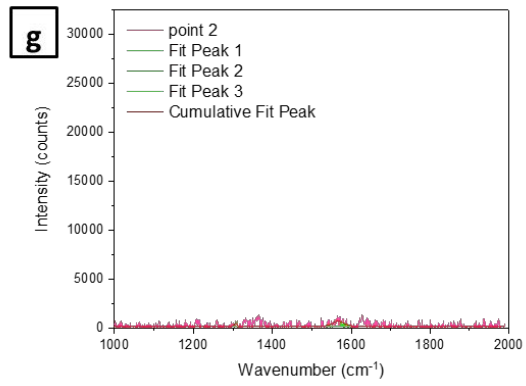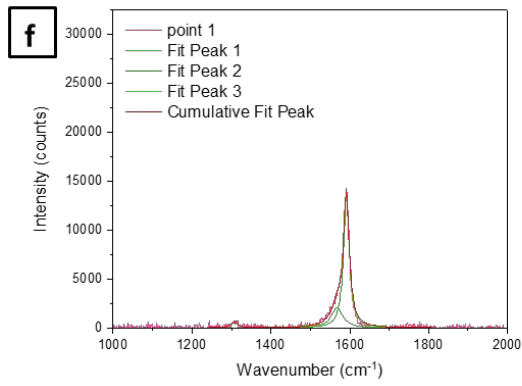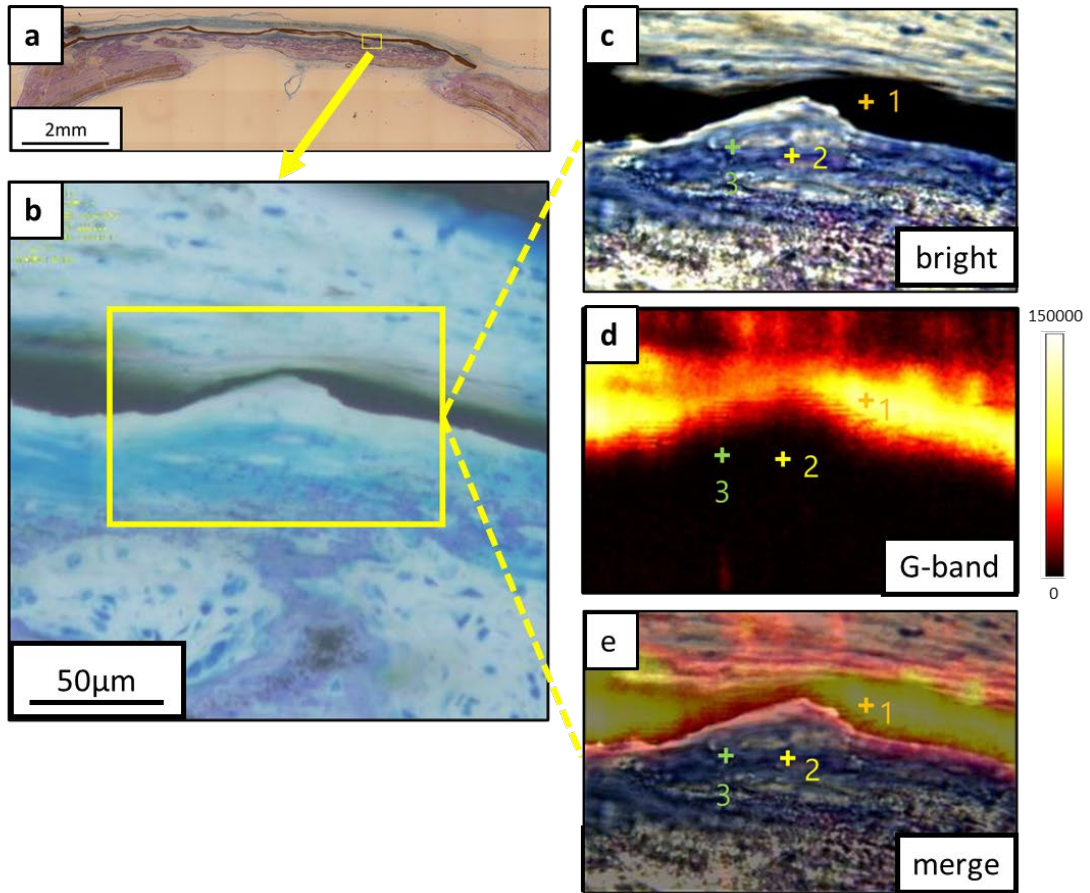
i	Center Max	FWHM	Max Height	Area Fit	Normalized %
Point 1 (CNT)	1591.6	16.9	13580.3	360805.2	100.0
Point 2	1580	15.1	171.5	4073.0	1.1
Point 3	1584.3	13.0	154.2	3149.0	0.9

Figure 5. (a) Histological sections of calvarial bone specimen implanted with HACNT membrane after 8 weeks. (b) High magnification of (a). (c)-(e) Raman imaging at high magnification of white square in (b). (c) bright field, (d) G-band field and (e)merge field under Raman microscope observation, 3 points were selected to detect CNTs. Graphs (f)-(h) are the intensity spectrum of excited at 785nm in 3 points. The intensity of CNTs was normalized to 100%. (f)Point 1 (CNT): 100%. (g)Point 2: 1.1%. (h)Point 3: 0.9%. Table (i) is the intensity of each point.

Acknowledgments

References

(1)   Iijima, S. Helical Microtubules of Graphitic Carbon. *Nature* **1991**, *354* (6348), 56–58. https://doi.org/10.1038/354056a0.

(2)   Iijima, S.; Ichihashi, T. Single-Shell Carbon Nanotubes of 1-Nm Diameter. *Nature* **1993**, *363* (6430), 603–605. https://doi.org/10.1038/363603a0.

(3)   Liu, X.; George, M. N.; Park, S.; Miller II, A. L.; Gaihre, B.; Li, L.; Waletzki, B. E.; Terzic, A.; Yaszemski, M. J.; Lu, L. 3D-Printed Scaffolds with Carbon Nanotubes for Bone Tissue Engineering: Fast and Homogeneous One-Step Functionalization. *Acta Biomater.* **2020**, *111*, 129–140. https://doi.org/10.1016/j.actbio.2020.04.047.

(4)   Patel, K. D.; Kim, T. H.; Mandakhbayar, N.; Singh, R. K.; Jang, J. H.; Lee, J. H.; Kim, H. W. Coating Biopolymer Nanofibers with Carbon Nanotubes Accelerates Tissue Healing and Bone Regeneration through Orchestrated Cell- and Tissue-Regulatory Responses. *Acta Biomater.* **2020**, *108*, 97–110. https://doi.org/10.1016/j.actbio.2020.03.012.

(5)   Peng, Z.; Zhao, T.; Zhou, Y.; Li, S.; Li, J.; Leblanc, R. M. Bone Tissue Engineering via Carbon-Based Nanomaterials. *Adv. Healthc. Mater.* **2020**, *9* (5), 1–30. https://doi.org/10.1002/adhm.201901495.

(6)   Huang, B.; Vyas, C.; Byun, J. J.; El-Newehy, M.; Huang, Z.; Bártolo, P. Aligned Multi-Walled Carbon Nanotubes with Nanohydroxyapatite in a 3D Printed Polycaprolactone Scaffold Stimulates Osteogenic Differentiation. *Mater. Sci. Eng. C* **2020**, *108* (July 2019), 110374. https://doi.org/10.1016/j.msec.2019.110374.

(7)   Genady, A. R.; Fong, D.; Slikboer, S. R.; El-Zaria, M. E.; Swann, R.; Janzen, N.; Faraday, A.; McNelles, S. A.; Rezvani, M.; Sadeghi, S.; Adronov, A.; Valliant, J. F. 99mTc-Functionalized Single-Walled Carbon Nanotubes for Bone Targeting. *ACS Appl. Nano Mater.* **2020**, *3* (12), 11819–11824. https://doi.org/10.1021/acsanm.0c02339.

(8)   Usui, Y.; Aoki, K.; Narita, N.; Murakami, N.; Nakamura, I.; Nakamura, K.; Ishigaki, N.; Yamazaki, H.; Horiuchi, H.; Kato, H.; Taruta, S.; Kim, Y. A.; Endo, M.; Saito, N. Carbon Nanotubes with High Bone-Tissue Compatibility and Bone-Formation Acceleration Effects. *Small* **2008**, *4* (2), 240–246. https://doi.org/10.1002/smll.200700670.

(9)   Barrientos-Durán, A.; Carpenter, E. M.; Zur Nieden, N. I.; Malinin, T. I.; Rodríguez-Manzaneque, J. C. arlo.; Zanello, L. P. Carboxyl-Modified Single-Wall Carbon Nanotubes Improve Bone Tissue Formation in Vitro and Repair in an in Vivo Rat Model. *Int. J. Nanomedicine* **2014**, *9*, 4277–4291. https://doi.org/10.2147/IJN.S62538.

(10)   Hirata, E.; Uo, M.; Takita, H.; Akasaka, T.; Watari, F.; Yokoyama, A. Multiwalled Carbon Nanotube-Coating of 3D Collagen Scaffolds for Bone Tissue Engineering.

Carbon N. Y. **2011**, *49* (10), 3284–3291. https://doi.org/10.1016/j.carbon.2011.04.002.

(11) Hirata, E.; Uo, M.; Nodasaka, Y.; Takita, H.; Ushijima, N.; Akasaka, T.; Watari, F.; Yokoyama, A. 3D Collagen Scaffolds Coated with Multiwalled Carbon Nanotubes: Initial Cell Attachment to Internal Surface. *J. Biomed. Mater. Res. - Part B Appl. Biomater.* **2010**, *93* (2), 544–550. https://doi.org/10.1002/jbm.b.31613.

(12) Hirata, E.; Uo, M.; Takita, H.; Akasaka, T.; Watari, F.; Yokoyama, A. Development of a 3D Collagen Scaffold Coated with Multiwalled Carbon Nanotubes. *J. Biomed. Mater. Res. - Part B Appl. Biomater.* **2009**, *90 B* (2), 629–634. https://doi.org/10.1002/jbm.b.31327.

(13) Hirata, E.; Ménard-Moyon, C.; Venturelli, E.; Takita, H.; Watari, F.; Bianco, A.; Yokoyama, A. Carbon Nanotubes Functionalized with Fibroblast Growth Factor Accelerate Proliferation of Bone Marrow-Derived Stromal Cells and Bone Formation. *Nanotechnology* **2013**, *24* (43), 435101. https://doi.org/10.1088/0957-4484/24/43/435101.

(14) Omar, O.; Elgali, I.; Dahlin, C.; Thomsen, P. Barrier Membranes: More than the Barrier Effect? *J. Clin. Periodontol.* **2019**, *46* (S21), 103–123. https://doi.org/10.1111/jcpe.13068.

(15) Dahlin, C.; Linde, A.; Gottlow, J.; Nyman, S. Healing of Bone Defects by Guided Tissue Regeneration. *Plast. Reconstr. Surg.* **1988**, *81* (5), 672–676. https://doi.org/10.1097/00006534-198805000-00004.

(16) Hämmerle, C. H. F.; Jung, R. E. Bone Augmentation by Means of Barrier Membranes. *Periodontol. 2000* **2003**, *33*, 36–53. https://doi.org/10.1046/j.0906-6713.2003.03304.x.

(17) Elgali, I.; Omar, O.; Dahlin, C.; Thomsen, P. Guided Bone Regeneration: Materials and Biological Mechanisms Revisited. *Eur. J. Oral Sci.* **2017**, *125* (5), 315–337. https://doi.org/10.1111/eos.12364.

(18) Kim, H. Y.; Park, J. H.; Byun, J. H.; Lee, J. H.; Oh, S. H. BMP-2-Immobilized Porous Matrix with Leaf-Stacked Structure as a Bioactive GBR Membrane. *ACS Appl. Mater. Interfaces* **2018**, *10* (36), 30115–30124. https://doi.org/10.1021/acsami.8b09558.

(19) Kasai, T.; Matsumura, S.; Iizuka, T.; Shiba, K.; Kanamori, T.; Yudasaka, M.; Iijima, S.; Yokoyama, A. Carbon Nanohorns Accelerate Bone Regeneration in Rat Calvarial Bone Defect. *Nanotechnology* **2011**, *22* (6), 065102. https://doi.org/10.1088/0957-4484/22/6/065102.

(20) Hirata, E.; Miyako, E.; Hanagata, N.; Ushijima, N.; Sakaguchi, N.; Russier, J.; Yudasaka, M.; Iijima, S.; Bianco, A.; Yokoyama, A. Carbon Nanohorns Allow Acceleration of Osteoblast Differentiation via Macrophage Activation. *Nanoscale* **2016**, *8* (30), 14514–14522. https://doi.org/10.1039/C6NR02756C.

(21) Iijima, S. Carbon Nanotubes: Past, Present, and Future. *Phys. B Condens. Matter* **2002**, *323* (1–4), 1–5. https://doi.org/10.1016/S0921-4526(02)00869-4.

(22)   Newman, P.; Minett, A.; Ellis-Behnke, R.; Zreiqat, H. Carbon Nanotubes: Their Potential and Pitfalls for Bone Tissue Regeneration and Engineering. *Nanomedicine Nanotechnology, Biol. Med.* **2013**, *9* (8), 1139–1158. https://doi.org/10.1016/j.nano.2013.06.001.

(23)   Kodama, H.; Amagai, Y.; Sudo, H.; Kasai, S.; Yamamoto, S. Establishment of a Clonal Osteogenic Cell Line from Newborn Mouse Calvaria. *Japanese J. Oral Biol.* **1981**, *23* (4), 899–901. https://doi.org/10.2330/joralbiosci1965.23.899.

(24)   Kaga, N.; Akasaka, T.; Matsuura, T.; Yokoyama, A.; Yoshida, Y. Proliferation of Saos-2 and Ca9-22 Cells on Grooved and Pillared Titanium Surfaces. *Biomed. Mater. Eng.* **2020**, *30* (5–6), 559–567. https://doi.org/10.3233/BME-191074.

(25)   TODARO, G. J.; GREEN, H. Quantitative Studies of the Growth of Mouse Embryo Cells in Culture and Their Development into Established Lines. *J. Cell Biol.* **1963**, *17* (6), 299–313. https://doi.org/10.1083/jcb.17.2.299.

(26)   Perez, M.; Fornell, P.; Garcia-Aznar, J.; Doblaré, M. Validation of Bone Remodelling Models Applied to Different Bone Types Using Mimics. **2007**, No. January 2016.

(27)   Takeuchi, T.; Iizumi, Y.; Yudasaka, M.; Kizaka-Kondoh, S.; Okazaki, T. Characterization and Biodistribution Analysis of Oxygen-Doped Single-Walled Carbon Nanotubes Used as in Vivo Fluorescence Imaging Probes. *Bioconjug. Chem.* **2019**, *30* (5), 1323–1330. https://doi.org/10.1021/acs.bioconjchem.9b00088.

(28)   Hemshekhar, M.; Thushara, R. M.; Chandranayaka, S.; Sherman, L. S.; Kemparaju, K.; Girish, K. S. Emerging Roles of Hyaluronic Acid Bioscaffolds in Tissue Engineering and Regenerative Medicine. *Int. J. Biol. Macromol.* **2016**, *86*, 917–928. https://doi.org/10.1016/j.ijbiomac.2016.02.032.

(29)   Schanté, C. E.; Zuber, G.; Herlin, C.; Vandamme, T. F. Chemical Modifications of Hyaluronic Acid for the Synthesis of Derivatives for a Broad Range of Biomedical Applications. *Carbohydr. Polym.* **2011**, *85* (3), 469–489. https://doi.org/10.1016/j.carbpol.2011.03.019.

(30)   Silva, C. R.; Babo, P. S.; Gulino, M.; Costa, L.; Oliveira, J. M.; Silva-Correia, J.; Domingues, R. M. A.; Reis, R. L.; Gomes, M. E. Injectable and Tunable Hyaluronic Acid Hydrogels Releasing Chemotactic and Angiogenic Growth Factors for Endodontic Regeneration. *Acta Biomater.* **2018**, *77*, 155–171. https://doi.org/10.1016/j.actbio.2018.07.035.

(31)   Kang, S.; Herzberg, M.; Rodrigues, D. F.; Elimelech, M. Antibacterial Effects of Carbon Nanotubes: Size Does Matter! *Langmuir* **2008**, *24* (13), 6409–6413. https://doi.org/10.1021/la800951v.

(32)   Padial-Molina, M.; Galindo-Moreno, P.; Fernández-Barbero, J. E.; O'Valle, F.; Jódar-Reyes, A. B.; Ortega-Vinuesa, J. L.; Ramón-Torregrosa, P. J. Role of Wettability and Nanoroughness on Interactions between Osteoblast and Modified

Silicon Surfaces. *Acta Biomater.* **2011**, *7* (2), 771–778. https://doi.org/10.1016/j.actbio.2010.08.024.

(33)   Hirata, E.; Yudasaka, M.; Ushijima, N.; Sakaguchi, N.; Maeda, Y.; Tanaka, T.; Kataura, H.; Yokoyama, A. Fate of Carbon Nanotubes Locally Implanted in Mice Evaluated by Near-Infrared Fluorescence Imaging: Implications for Tissue Regeneration. *ACS Appl. Nano Mater.* **2019**, *2* (3), 1382–1390. https://doi.org/10.1021/acsanm.8b02267.

(34)   van Kooten, T. G.; Schakenraad, J. M.; van der Mei, H. C.; Busscher, H. J. Influence of Substratum Wettability on the Strength of Adhesion of Human Fibroblasts. *Biomaterials* **1992**, *13* (13), 897–904. https://doi.org/10.1016/0142-9612(92)90112-2.

(35)   Foraida, Z. I.; Kamaldinov, T.; Nelson, D. A.; Larsen, M.; Castracane, J. Elastin-PLGA Hybrid Electrospun Nanofiber Scaffolds for Salivary Epithelial Cell Self-Organization and Polarization. *Acta Biomater.* **2017**, *62*, 116–127. https://doi.org/10.1016/j.actbio.2017.08.009.

(36)   Zhang, J.; Li, J.; Han, Y. Superhydrophobic PTFE Surfaces by Extension. *Macromol. Rapid Commun.* **2004**, *25* (11), 1105–1108. https://doi.org/10.1002/marc.200400065.

(37)   Ribeiro, N.; Sousa, S. R.; Monteiro, F. J. Influence of Crystallite Size of Nanophased Hydroxyapatite on Fibronectin and Osteonectin Adsorption and on MC3T3-E1 Osteoblast Adhesion and Morphology. *J. Colloid Interface Sci.* **2010**, *351* (2), 398–406. https://doi.org/10.1016/j.jcis.2010.08.013.

(38)   Toffoli, A.; Parisi, L.; Bianchi, M. G.; Lumetti, S.; Bussolati, O.; Macaluso, G. M. Thermal Treatment to Increase Titanium Wettability Induces Selective Proteins Adsorption from Blood Serum Thus Affecting Osteoblasts Adhesion. *Mater. Sci. Eng. C* **2020**, *107* (August 2019). https://doi.org/10.1016/j.msec.2019.110250.

(39)   Kunzler, T. P.; Drobek, T.; Schuler, M.; Spencer, N. D. Systematic Study of Osteoblast and Fibroblast Response to Roughness by Means of Surface-Morphology Gradients. *Biomaterials* **2007**, *28* (13), 2175–2182. https://doi.org/10.1016/j.biomaterials.2007.01.019.

(40)   Baharloo, B.; Textor, M.; Brunette, D. M. Substratum Roughness Alters the Growth, Area, and Focal Adhesions of Epithelial Cells, and Their Proximity to Titanium Surfaces. *J. Biomed. Mater. Res. - Part A* **2005**, *74* (1), 12–22. https://doi.org/10.1002/jbm.a.30321.